Implicit Application of Non-Reflective Boundary Conditions for Navier-Stokes Equations in Generalized Coordinates

Xiangying Chen* and Ge-Cheng Zha†
Dept. of Mechanical and Aerospace Engineering
University of Miami
Coral Gables, Florida 33124
xychen@apollo.eng.miami.edu,
zha@apollo.eng.miami.edu

Abstract

The non-reflective boundary conditions for Navier-Stokes equations originally suggested by Poinsot and Lele[1] in Cartesian coordinates are extended to generalized coordinates. The boundary conditions are implicitly coupled with the Navier-Stokes flow solver in the inner domain. The calculations are conducted for a subsonic vortex propagating flow and the steady and unsteady transonic inlet-diffuser flows. The results indicate that the present method is accurate and robust, and the non-reflective boundary conditions are essential for unsteady flow calculations.

1 Introduction

The accuracy of unsteady flow calculations relies on accurate treatment of boundary conditions. Due to the computer resource limit, usually only a limited computational domain is considered for an unsteady flow calculation. This means that we have to "cut off" the domain that is not of our primary interest. However, the cut boundaries may cause artificial wave reflections, which may include both physical waves and numerical waves[1]. Such waves may bounce back and forth within the computational domain and may seriously contaminate the solutions and produce misleading results. This is particularly true for internal flows such as the flows in turbomachinery, in which the computational domain usually is confined very near the solid objects. For example, previous studies indicated that the different treatment of perturbation at upstream and downstream boundaries can change the compressor blade stall inception pattern [2] [3].

The currently often used non-reflective boundary conditions for unsteady internal flows are based on eigenvalue analysis of linearized Euler equations developed by Giles[4]. However, Giles' method may only apply to the inviscid solutions which require the far field flow to be uniform so that

* Post Doctoral Associate
† Associate Professor

the propagation waves have the Fourier mode shapes. For viscous flows, the mean flow in the downstream far field region may be non-uniform due to the airfoil or blade wakes, which means that there will be no Fourier mode shapes. In addition, the inconsistency of the Navier-Stokes governing equations for the inner domain and linearized Euler equations at far field boundary may also cause numerical wave reflections.

The more rigorous treatment of non-reflective boundary conditions (NRBC) for Navier-Stokes equations is the one suggested by Poinsot and Lele in 1992[1] for Direct Numerical Simulation of turbulence. However, the NRBC given by Poinsot and Lele in [1] is only for the regular mesh aliened with the coordinate axises in Cartesian coordinates. The explicit time marching scheme was used in the calculation of Poinsot and Lele. For practical engineering applications, the body fitted generalized coordinates are usually used. In 2000, Kim and Lee [5] made an effort to extend the NRBC of Poinsot and Lele from the Cartesian coordinates to generalized coordinates. However, in their derivation, a flaw was made by absorbing the eigenvector matrix into the partial derivatives, which apply only if: 1) it is 1D equations; 2) the eigenvector matrix is constant in the flow field; 3) the partial differential equations satisfy Pfaff's condition. For multidimensional Navier-Stokes equations, all these three conditions are not satisfied[6, 7]. Hence, the wave amplitude vector derived in [5] is erroneous.

The purpose of this paper is to extend the NRBC of Poinsot and Lele [1] from Cartesian coordinates to generalized coordinates and apply it numerically for unsteady calculations in an implicit time marching method. The numerical results indicate that the present methodology is robust and accurate.

2 Governing Equations

The 3D compressible Reynolds-Averaged Navier-Stokes equations (RANS) with Favre mass average are solved for the flow field in generalized coordinates, which can be expressed as

$$\frac{\partial \mathbf{Q}'}{\partial t} + \frac{\partial \mathbf{E}'}{\partial \xi} + \frac{\partial \mathbf{F}'}{\partial \eta} + \frac{\partial \mathbf{G}'}{\partial \zeta} = \frac{1}{Re}\left(\frac{\partial \mathbf{E}'_{\mathbf{v}}}{\partial \xi} + \frac{\partial \mathbf{F}'_{\mathbf{v}}}{\partial \eta} + \frac{\partial \mathbf{G}'_{\mathbf{v}}}{\partial \zeta}\right) \tag{1}$$

where Re is the Reynolds number and

$$\mathbf{Q}' = \frac{\mathbf{Q}}{J} \tag{2}$$

$$\mathbf{E}' = \frac{1}{J}(\xi_x \mathbf{E} + \xi_y \mathbf{F} + \xi_z \mathbf{G}) \tag{3}$$

$$\mathbf{F}' = \frac{1}{J}(\eta_x \mathbf{E} + \eta_y \mathbf{F} + \eta_z \mathbf{G}) \tag{4}$$

$$\mathbf{G}' = \frac{1}{J}(\zeta_x \mathbf{E} + \zeta_y \mathbf{F} + \zeta_z \mathbf{G}) \tag{5}$$

$$\mathbf{E}'_{\mathbf{v}} = \frac{1}{J}(\xi_x \mathbf{E}_{\mathbf{v}} + \xi_y \mathbf{F}_{\mathbf{v}} + \xi_z \mathbf{G}_{\mathbf{v}}) \tag{6}$$

$$\mathbf{F}'_{\mathbf{v}} = \frac{1}{J}(\eta_x \mathbf{E}_{\mathbf{v}} + \eta_y \mathbf{F}_{\mathbf{v}} + \eta_z \mathbf{G}_{\mathbf{v}}) \tag{7}$$

$$\mathbf{G}'_{\mathbf{v}} = \frac{1}{J}(\zeta_x \mathbf{E}_{\mathbf{v}} + \zeta_y \mathbf{F}_{\mathbf{v}} + \zeta_z \mathbf{G}_{\mathbf{v}}) \tag{8}$$

where the variable vector $\mathbf{Q}$, and inviscid flux vectors $\mathbf{E}$, $\mathbf{F}$, and $\mathbf{G}$ are

$$\mathbf{Q} = \begin{pmatrix} \bar{\rho} \\ \bar{\rho}\tilde{u} \\ \bar{\rho}\tilde{v} \\ \bar{\rho}\tilde{w} \\ \bar{\rho}\tilde{e} \end{pmatrix}, \mathbf{E} = \begin{pmatrix} \bar{\rho}\tilde{u} \\ \bar{\rho}\tilde{u}\tilde{u} + \tilde{p} \\ \bar{\rho}\tilde{u}\tilde{v} \\ \bar{\rho}\tilde{u}\tilde{w} \\ (\bar{\rho}\tilde{e} + \tilde{p})\tilde{u} \end{pmatrix}, \mathbf{F} = \begin{pmatrix} \bar{\rho}\tilde{v} \\ \bar{\rho}\tilde{u}\tilde{v} \\ \bar{\rho}\tilde{v}\tilde{v} + \tilde{p} \\ \bar{\rho}\tilde{w}\tilde{v} \\ (\bar{\rho}\tilde{e} + \tilde{p})\tilde{v} \end{pmatrix}, \mathbf{G} = \begin{pmatrix} \bar{\rho}w \\ \bar{\rho}\tilde{u}\tilde{w} \\ \bar{\rho}\tilde{v}\tilde{w} \\ \bar{\rho}\tilde{w}\tilde{w} + \tilde{p} \\ (\bar{\rho}\tilde{e} + \tilde{p})\tilde{w} \end{pmatrix},$$

and the viscous flux vectors are given by

$$\mathbf{E}_{\mathbf{v}} = \begin{pmatrix} 0 \\ \bar{\tau}_{xx} - \overline{\rho u'' u''} \\ \bar{\tau}_{xy} - \overline{\rho u'' v''} \\ \bar{\tau}_{xz} - \overline{\rho u'' w''} \\ Q_x \end{pmatrix}, \mathbf{F}_{\mathbf{v}} = \begin{pmatrix} 0 \\ \bar{\tau}_{yx} - \overline{\rho v'' u''} \\ \bar{\tau}_{yy} - \overline{\rho v'' v''} \\ \bar{\tau}_{yz} - \overline{\rho v'' w''} \\ Q_y \end{pmatrix}, \mathbf{G}_{\mathbf{v}} = \begin{pmatrix} 0 \\ \bar{\tau}_{zx} - \overline{\rho w'' u''} \\ \bar{\tau}_{zy} - \overline{\rho w'' v''} \\ \bar{\tau}_{zz} - \overline{\rho w'' w''} \\ Q_z \end{pmatrix}$$

In above equations, ρ is the density, u, v, and w are the Cartesian velocity components in x, y and z directions, p is the static pressure, and e is the total energy per unit mass. The overbar denotes the Reynolds-averaged quantity, tilde and double-prime denote the Favre mean and Favre fluctuating part of the turbulent motion respectively. All the flow variables in above equations are normalized by using the freestream quantities and the reference length L.

Let subscript 1, 2 and 3 represent the coordinates, x, y, and z, and use Einstein summation convention, the non-dimensional shear-stress and Q_x, Q_y, Q_z terms can be expressed in tensor form as

$$\bar{\tau}_{ij} = -\frac{2}{3}\tilde{\mu}\frac{\partial \tilde{u}_k}{\partial x_k}\delta_{ij} + \tilde{\mu}(\frac{\partial \tilde{u}_i}{\partial x_j} + \frac{\partial \tilde{u}_j}{\partial x_i}) \tag{9}$$

$$Q_i = \tilde{u}_j(\bar{\tau}_{ij} - \overline{\rho u_i'' u_j''}) - (\bar{q}_i + C_p\overline{\rho T'' u_i''}) \tag{10}$$

where the mean molecular heat flux is

$$\bar{q}_i = -\frac{\tilde{\mu}}{(\gamma - 1)Pr}\frac{\partial a^2}{\partial x_i} \tag{11}$$

The molecular viscosity $\tilde{\mu} = \tilde{\mu}(\tilde{T})$ is determined by Sutherland law, and $a = \sqrt{\gamma R T_\infty}$ is the speed of sound. The equation of state closes the system,

$$\bar{\rho}\tilde{e} = \frac{\tilde{p}}{(\gamma - 1)} + \frac{1}{2}\bar{\rho}(\tilde{u}^2 + \tilde{v}^2 + \tilde{w}^2) + k \tag{12}$$

where γ is the ratio of specific heats, k is the Favre mass-averaged turbulence kinetic energy. The turbulent shear stresses and heat flux appeared in above equations are calculated by Baldwin-Lomax model[8]. The viscosity is composed of $\mu + \mu_t$, where μ is the molecular viscosity and μ_t is the turbulent viscosity determined by Baldwin Lomax model. For a laminar flow, the μ_t is set to be zero. For simplicity, the overbars and tildes are dropped in later analysis.

2.1 Time Marching Scheme

For the inner flow field domain, the Navier-Stokes equations, Equation (1), are solved implicitly using the control volume method. For steady state solutions, the original Navier-Stokes equations, Equation (1), are solved. For unsteady flow calculations, the dual time stepping method suggested by Jameson is used[9] with a pseudo temporal term $\frac{\partial \mathbf{Q}}{\partial \tau}$ added to the governing equations. This term vanishes at the end of each physical time step and has no influence on the accuracy of the solution. However, instead of using the explicit scheme as in [9], an implicit pseudo time marching scheme using line Gauss-Seidel iteration is employed to achieve high CPU efficiency. For unsteady time accurate computations, the temporal term is discretized implicitly using a three point, backward differencing as the following

$$\frac{\partial \mathbf{Q}}{\partial t} = \frac{3Q^{n+1} - 4Q^n + Q^{n-1}}{2\Delta t} \tag{13}$$

where n is the time level index. The pseudo temporal term is discretized with first order Euler scheme. Let m stand for the iteration index within a physical time step, the semi-discretized governing equation (eq.(1)) can be expressed as

$$\left[\left(\frac{1}{\Delta\tau} + \frac{1.5}{\Delta t}\right) I - \left(\frac{\partial R}{\partial Q}\right)^{n+1,m}\right] \delta Q^{n+1,m+1} = R^{n+1,m} - \frac{3Q^{n+1,m} - 4Q^n + Q^{n-1}}{2\Delta t} \tag{14}$$

where the $\Delta\tau$ is the pseudo time step, R is the net flux going through the control volume,

$$R = -\frac{1}{V}\int_s [(\mathbf{E}' - \frac{1}{Re}\mathbf{E}'_v)\mathbf{i} + (\mathbf{F}' - \frac{1}{Re}\mathbf{F}'_v)\mathbf{j} + (\mathbf{G}' - \frac{1}{Re}\mathbf{G}'_v)\mathbf{k}]\cdot d\mathbf{s} \tag{15}$$

where V is the volume of the control volume, $\mathbf{s}$ is the control volume surface area vector. Equation (14) is solved using the unfactored line Gauss-Seidel iteration. The method can reach very large pseudo time step since no factorization error is introduced.

To resolve the shock wave and wall boundary layer with high accuracy, the Roe scheme [10] is employed to evaluate the inviscid fluxes with the 3rd order MUSCL type differencing[11]. Central differencing is used for viscous fluxes calculation.

3 Characteristic Form of the Navier-Stokes Equations

The characteristic form of the Navier-Stokes equations in the generalized coordinates will be solved as the non-reflective boundary conditions. To describe the derivation process, the ξ direction will be taken as the example. Other two directions can follow the same procedure. Based on the strategy of Thompson[7] and Poinsot and Lele[1], the Navier-Stokes equations are expressed first using primitive variables as the following:

$$\mathbf{M}\frac{\partial \mathbf{q}}{\partial t} + \mathbf{A}\cdot\mathbf{M}\frac{\partial \mathbf{q}}{\partial \xi} + \mathbf{B}\cdot\mathbf{M}\frac{\partial \mathbf{q}}{\partial \eta} + \mathbf{C}\cdot\mathbf{M}\frac{\partial \mathbf{q}}{\partial \zeta} = \mathbf{R_v} \tag{16}$$

where $\mathbf{A}, \mathbf{B}, \mathbf{C}$ are the Jacobian matrix

$$\mathbf{A} = \frac{\partial \mathbf{E}'}{\partial \mathbf{Q}'}, \mathbf{B} = \frac{\partial \mathbf{F}'}{\partial \mathbf{Q}'}, \mathbf{C} = \frac{\partial \mathbf{G}'}{\partial \mathbf{Q}'} \tag{17}$$

where $\mathbf{R_v}$ is the viscous vector on the right hand side of the Navier-Stokes equations, (Equation (1)), $\mathbf{q}$ is the primitive variable vector:

$$\mathbf{q} = \frac{1}{J}\begin{pmatrix} \rho \\ u \\ v \\ w \\ p \end{pmatrix} \tag{18}$$

$\mathbf{M}$ is the Jacobian matrix between the conservative variables and primitive variables

$$\mathbf{M} = \frac{\partial \mathbf{Q}'}{\partial \mathbf{q}} = \begin{pmatrix} 1 & 0 & 0 & 0 & 0 \\ u & \rho & 0 & 0 & 0 \\ v & 0 & \rho & 0 & 0 \\ w & 0 & 0 & \rho & 0 \\ \frac{\Phi}{\gamma-1} & \rho u & \rho v & \rho w & \frac{1}{\gamma-1} \end{pmatrix} \tag{19}$$

where $\Phi = \frac{\gamma-1}{2}(u^2 + v^2 + w^2)$.

Equation (16) can be further expressed as:

$$\frac{\partial \mathbf{q}}{\partial t} + \mathbf{a}\frac{\partial \mathbf{q}}{\partial \xi} + \mathbf{b}\frac{\partial \mathbf{q}}{\partial \eta} + \mathbf{c}\frac{\partial \mathbf{q}}{\partial \zeta} = \mathbf{M^{-1}R_v} \tag{20}$$

Where

$$\mathbf{a} = \mathbf{M^{-1}AM}, \mathbf{b} = \mathbf{M^{-1}BM}, \mathbf{c} = \mathbf{M^{-1}CM} \tag{21}$$

$$\mathbf{M^{-1}} = \begin{pmatrix} 1 & 0 & 0 & 0 & 0 \\ -\frac{u}{\rho} & \frac{1}{\rho} & 0 & 0 & 0 \\ -\frac{v}{\rho} & 0 & \frac{1}{\rho} & 0 & 0 \\ -\frac{w}{\rho} & 0 & 0 & \frac{1}{\rho} & 0 \\ \Phi & -u(\gamma-1) & -v(\gamma-1) & -w(\gamma-1) & \gamma-1 \end{pmatrix} \tag{22}$$

Matrix $\mathbf{a}, \mathbf{b}, \mathbf{c}$ have the same eigenvalues as Jacobian matrix $\mathbf{A}, \mathbf{B}, \mathbf{C}$. In ξ direction,

$$\mathbf{a} = \begin{pmatrix} U & \rho\xi_x & \rho\xi_y & \rho\xi_z & 0 \\ 0 & U & 0 & 0 & \frac{\xi_x}{\rho} \\ 0 & 0 & U & 0 & \frac{\xi_y}{\rho} \\ 0 & 0 & 0 & U & \frac{\xi_z}{\rho} \\ 0 & \gamma p\xi_x & \gamma p\xi_y & \gamma p\xi_z & U \end{pmatrix} \tag{23}$$

where $U = \xi_x u + \xi_y v + \xi_z w$. Matrix $\mathbf{a}$ can also be expressed as

$$\mathbf{a} = \mathbf{P}\mathbf{\Lambda}\mathbf{P}^{-1} \tag{24}$$

where $\mathbf{\Lambda}$ is the eigenvalue matrix, $\mathbf{P}$ is eigenvector matrix of $\mathbf{a}$, and $\mathbf{P^{-1}}$ is the inverse of $\mathbf{P}$. They are given as the following

$$\mathbf{\Lambda} = \begin{pmatrix} U & 0 & 0 & 0 & 0 \\ 0 & U & 0 & 0 & 0 \\ 0 & 0 & U & 0 & 0 \\ 0 & 0 & 0 & U+C & 0 \\ 0 & 0 & 0 & 0 & U-C \end{pmatrix} \tag{25}$$

$$\mathbf{P} = \begin{pmatrix} \tilde{\xi}_x & \tilde{\xi}_y & \tilde{\xi}_z & \alpha & \alpha \\ 0 & -\tilde{\xi}_z & \tilde{\xi}_y & \tilde{\xi}_x/\sqrt{2} & -\tilde{\xi}_x/\sqrt{2} \\ \tilde{\xi}_z & 0 & -\tilde{\xi}_x & \tilde{\xi}_y/\sqrt{2} & -\tilde{\xi}_y/\sqrt{2} \\ -\tilde{\xi}_y & \tilde{\xi}_x & 0 & \tilde{\xi}_z/\sqrt{2} & -\tilde{\xi}_z/\sqrt{2} \\ 0 & 0 & 0 & \alpha c^2 & \alpha c^2 \end{pmatrix} \tag{26}$$

$$\mathbf{P^{-1}} = \begin{pmatrix} \tilde{\xi}_x & 0 & \tilde{\xi}_z & -\tilde{\xi}_y & -\tilde{\xi}_x/c^2 \\ \tilde{\xi}_y & -\tilde{\xi}_z & 0 & \tilde{\xi}_x & -\tilde{\xi}_y/c^2 \\ \tilde{\xi}_z & \tilde{\xi}_y & -\tilde{\xi}_x & 0 & -\tilde{\xi}_z/c^2 \\ 0 & \tilde{\xi}_x/\sqrt{2} & \tilde{\xi}_y/\sqrt{2} & \tilde{\xi}_z/\sqrt{2} & \beta \\ 0 & -\tilde{\xi}_x/\sqrt{2} & -\tilde{\xi}_y/\sqrt{2} & -\tilde{\xi}_z/\sqrt{2} & \beta \end{pmatrix} \tag{27}$$

where $C = c\beta_\xi$, $\beta_\xi = \sqrt{{\xi_x}^2 + {\xi_y}^2 + {\xi_z}^2}$, $\tilde{\xi}_x = \xi_x/\beta_\xi$, $\tilde{\xi}_y = \xi_y/\beta_\xi$, and $\tilde{\xi}_z = \xi_z/\beta_\xi$, $\alpha = \rho/\sqrt{2}c$, and $\beta = 1/\sqrt{2}\rho c$, c is the speed of sound determined by $c = \sqrt{\gamma RT}$.

The Navier-Stokes equation, Equation (20) then can be expressed as:

$$\frac{\partial \mathbf{q}}{\partial t} + \mathbf{P}\mathbf{\Lambda}\mathbf{P}^{-1}\frac{\partial \mathbf{q}}{\partial \xi} + \mathbf{b}\frac{\partial \mathbf{q}}{\partial \eta} + \mathbf{c}\frac{\partial \mathbf{q}}{\partial \zeta} = \mathbf{M^{-1}R_v} \tag{28}$$

or

$$\mathbf{P^{-1}}\frac{\partial \mathbf{q}}{\partial t} + \mathbf{\Lambda}\mathbf{P}^{-1}\frac{\partial \mathbf{q}}{\partial \xi} + \mathbf{P^{-1}b}\frac{\partial \mathbf{q}}{\partial \eta} + \mathbf{P^{-1}c}\frac{\partial \mathbf{q}}{\partial \zeta} = \mathbf{P^{-1}M^{-1}R_v} \tag{29}$$

This is the characteristic form of the Navier-Stokes equations in ξ direction. Define vector $\mathcal{L}$ as:

$$\mathcal{L} = \mathbf{\Lambda P^{-1}} \frac{\partial \mathbf{q}}{\partial \xi} \tag{30}$$

The Navier-Stokes equations (Equation (29)) are then expressed as:

$$\mathbf{P^{-1}} \frac{\partial \mathbf{q}}{\partial t} + \mathcal{L} + \mathbf{P^{-1} b} \frac{\partial \mathbf{q}}{\partial \eta} + \mathbf{P^{-1} c} \frac{\partial \mathbf{q}}{\partial \zeta} = \mathbf{P^{-1} M^{-1} R_v} \tag{31}$$

Vector $\mathcal{L}$ is given as the following:

$$\mathcal{L} = \begin{pmatrix} \mathcal{L}_1 \\ \mathcal{L}_2 \\ \mathcal{L}_3 \\ \mathcal{L}_4 \\ \mathcal{L}_5 \end{pmatrix} = \begin{pmatrix} U[\tilde{\xi}_x \frac{\partial}{\partial \xi}(\frac{\rho}{J}) + \tilde{\xi}_z \frac{\partial}{\partial \xi}(\frac{v}{J}) - \tilde{\xi}_y \frac{\partial}{\partial \xi}(\frac{w}{J}) - \frac{\tilde{\xi}_x}{c^2} \frac{\partial}{\partial \xi}(\frac{p}{J})] \\ U[\tilde{\xi}_y \frac{\partial}{\partial \xi}(\frac{\rho}{J}) - \tilde{\xi}_z \frac{\partial}{\partial \xi}(\frac{u}{J}) + \tilde{\xi}_x \frac{\partial}{\partial \xi}(\frac{w}{J}) - \frac{\tilde{\xi}_y}{c^2} \frac{\partial}{\partial \xi}(\frac{p}{J})] \\ U[\tilde{\xi}_z \frac{\partial}{\partial \xi}(\frac{\rho}{J}) + \tilde{\xi}_y \frac{\partial}{\partial \xi}(\frac{u}{J}) - \tilde{\xi}_x \frac{\partial}{\partial \xi}(\frac{v}{J}) - \frac{\tilde{\xi}_z}{c^2} \frac{\partial}{\partial \xi}(\frac{p}{J})] \\ (U+C)[\frac{\tilde{\xi}_x}{\sqrt{2}} \frac{\partial}{\partial \xi}(\frac{u}{J}) + \frac{\tilde{\xi}_y}{\sqrt{2}} \frac{\partial}{\partial \xi}(\frac{v}{J}) + \frac{\tilde{\xi}_z}{\sqrt{2}} \frac{\partial}{\partial \xi}(\frac{w}{J}) + \beta \frac{\partial}{\partial \xi}(\frac{p}{J})] \\ (U-C)[-\frac{\tilde{\xi}_x}{\sqrt{2}} \frac{\partial}{\partial \xi}(\frac{u}{J}) - \frac{\tilde{\xi}_y}{\sqrt{2}} \frac{\partial}{\partial \xi}(\frac{v}{J}) - \frac{\tilde{\xi}_z}{\sqrt{2}} \frac{\partial}{\partial \xi}(\frac{w}{J}) + \beta \frac{\partial}{\partial \xi}(\frac{p}{J})] \end{pmatrix} \tag{32}$$

The vector $\mathcal{L}$ is the amplitude of the characteristic waves. If assume $\tilde{\xi}_x = 1, \tilde{\xi}_y = \tilde{\xi}_z = 0$, Equation (32) returns to the corresponding formulations in x-direction of the Cartesian coordinates.

As pointed out in [6, 7], for multi-dimensional Navier-Stokes flow equations, Equation (29), the matrix $\mathbf{P^{-1}}$ can not be absorbed into the partial derivatives because the flow equations does not satisfy Pfaff's condition and the matrix can not be treated as constants. In other words, it is incorrect to express the characteristic form of the Navier-Stokes equations in the form given in [5] (page 2042) as:

$$\frac{\partial \mathbf{R}}{\partial t} + \mathbf{\Lambda} \frac{\partial \mathbf{R}}{\partial \xi} + = \mathbf{P^{-1}} S_v^* \tag{33}$$

The local one-dimensional wave amplitude defined in [5] following Equation (33) is therefore also erroneous.

To be consistent with the governing equations of the flow field within inner domain and facilitate programming, it is desirable to express Equation (31) in terms of conservative variables. Multiply Equation (31) by matrix $\mathbf{M} \cdot \mathbf{P}$, the characteristic Navier-Stokes equations expressed in terms of conservative variables in ξ direction is:

$$\frac{\partial \mathbf{Q'}}{\partial t} + \mathbf{MP}\mathcal{L} + \frac{\partial \mathbf{F'}}{\partial \eta} + \frac{\partial \mathbf{G'}}{\partial \zeta} = \frac{1}{Re} \left(\frac{\partial \mathbf{E'_v}}{\partial \xi} + \frac{\partial \mathbf{F'_v}}{\partial \eta} + \frac{\partial \mathbf{G'_v}}{\partial \zeta} \right) \tag{34}$$

Define vector d as

$$d = \mathbf{P}\mathcal{L} = \begin{pmatrix} d_1 \\ d_2 \\ d_3 \\ d_4 \\ d_5 \end{pmatrix} = \begin{pmatrix} \tilde{\xi}_x \mathcal{L}_1 + \tilde{\xi}_y \mathcal{L}_2 + \tilde{\xi}_z \mathcal{L}_3 + \alpha(\mathcal{L}_4 + \mathcal{L}_5) \\ -\tilde{\xi}_z \mathcal{L}_2 + \tilde{\xi}_y \mathcal{L}_3 + \frac{\tilde{\xi}_x}{\sqrt{2}}(\mathcal{L}_4 - \mathcal{L}_5) \\ \tilde{\xi}_z \mathcal{L}_1 - \tilde{\xi}_x \mathcal{L}_3 + \frac{\tilde{\xi}_y}{\sqrt{2}}(\mathcal{L}_4 - \mathcal{L}_5) \\ -\tilde{\xi}_y \mathcal{L}_1 - \tilde{\xi}_x \mathcal{L}_2 + \frac{\tilde{\xi}_z}{\sqrt{2}}(\mathcal{L}_4 - \mathcal{L}_5) \\ \alpha c^2 (\mathcal{L}_4 + \mathcal{L}_5) \end{pmatrix} \tag{35}$$

Define vector $\mathcal{D}$ as:

$$\mathcal{D} = \mathbf{M}d = \begin{pmatrix} d_1 \\ ud_1 + \rho d_2 \\ vd_1 + \rho d_3 \\ wd_1 + \rho d_4 \\ \frac{1}{2}(u^2 + v^2 + w^2)d_1 + \rho u d_2 + \rho v d_3 + \rho w d_4 + \frac{1}{\gamma - 1} d_5 \end{pmatrix} \tag{36}$$

Finally the Navier-Stokes equations in generalized coordinates and their characteristic form in ξ direction can be expressed as:

$$\frac{\partial \mathbf{Q}'}{\partial t} + \mathcal{D} + \frac{\partial \mathbf{F}'}{\partial \eta} + \frac{\partial \mathbf{G}'}{\partial \zeta} = \frac{1}{Re} \left(\frac{\partial \mathbf{E}'_{\mathbf{v}}}{\partial \xi} + \frac{\partial \mathbf{F}'_{\mathbf{v}}}{\partial \eta} + \frac{\partial \mathbf{G}'_{\mathbf{v}}}{\partial \zeta} \right) \tag{37}$$

Equation (37) will be solved as the non-reflective boundary conditions in ξ direction. The Navier-Stokes equations in generalized coordinates and their characteristic forms in η and ζ directions can be obtained straightforwardly following the symmetric rule.

By neglecting the transverse and viscous terms in Equation (37), the Local One-Dimensional Inviscid (LODI) relation [1] in generalized coordinates is

$$\frac{\partial \mathbf{Q}'}{\partial t} + \mathcal{D} = 0 \tag{38}$$

The LODI relation may be used to estimate the amplitudes of the characteristic waves at boundaries. Numerical results show that the LODI relations works well for the boundaries where the flow fields are smooth or uniform, and hence the transverse and viscous terms are small or negligible. For those boundaries where the transverse and viscous terms are significant, the LODI relations may perform poorly.

4 Non-Reflective Boundary Conditions

Following the strategy suggested by Poinsot and Lele[1], the characteristic boundary conditions for Navier-Stokes equations can be implemented based on Equation (37). In the present study, Equation (37) is solved implicitly in a fully coupled way with the Navier-Stokes equations in inner domain. For unsteady solutions, the dual time stepping method is used. The semi-discretized equation for Equation (37) is:

$$\begin{aligned} &\left[\left(\frac{1}{\Delta \tau} + \frac{1.5}{\Delta t} \right) I - \left(\frac{\partial R_{bc}}{\partial Q} \right)^{n+1,m} + \left(\frac{\partial \mathcal{D}}{\partial Q} \right)^{n+1,m} \right] \delta Q^{n+1,m+1} \\ &= R_{bc}^{n+1,m} - \mathcal{D}^{n+1,m} - \frac{3Q^{n+1,m} - 4Q^n + Q^{n-1}}{2\Delta t} \end{aligned} \tag{39}$$

where

$$R_{bc} = -\frac{1}{V} \int_s [(-\frac{1}{Re}\mathbf{E}'_v)\mathbf{i} + (\mathbf{F}' - \frac{1}{Re}\mathbf{F}'_v)\mathbf{j} + (\mathbf{G}' - \frac{1}{Re}\mathbf{G}'_v)\mathbf{k}] \cdot d\mathbf{s} \tag{40}$$

Compare eq.(40) and (15), it is noticed that in R_{bc}, there is no $\mathbf{E}'$ flux, which is replaced by vector $\mathcal{D}$. $\mathcal{D}$ is treated as a source term.

Before proceeding to the further analysis, some notations need to be defined. For the finite volume method used in the present study, a row of phantom cells are used outside of the boundary. The boundary conditions are enforced by assigning values to the primitive variables at those phantom cells. All the variables marked by the subscript 'o' are for phantom cells. The variables at the interior cells adjacent to a boundary are denoted by subscript 'i'.

Equation (37) provides the set of governing equations for NRBC, but the way to implement the NRBC is not unique. The following is the method used in this study and should not be considered as the only feasible method.

4.1 Supersonic outflow boundary conditions

For supersonic flow at exit, all the eigenvalues in Equation (25) are positive and the disturbance propagates from inner domain to outside. The wave amplitude vector Equation (32) is evaluated using one side upwind differencing. For supersonic flow at exit, using simple extrapolation may not generate physical wave reflection, but may still generate numerical wave reflection[1]. Solving Equation (39) would achieve a more accurate non-reflective boundary conditions for the supersonic flow. For supersonic flow, the exit boundary conditions, ρ_o, ρu_o, ρv_o, ρw_o and ρe_o are completely determined by solving the Navier-Stokes equations in the characteristic form.

To evaluate the derivatives in vector $\mathcal{L}$, either the first order or second order upwind differencing may be used. For the present study, all the partial derivatives in vector $\mathcal{L}$ are calculated by first order upwind differencing.

4.2 Subsonic outflow boundary conditions

For subsonic flow at exit, the eigenvalue $U - C$ is negative and the disturbance propagates into the domain from outside. $\mathcal{L}_1$ to $\mathcal{L}_4$ can be still calculated by one-side upwind differencing. However, $\mathcal{L}_5$ corresponding to the eigenvalue of $U - C$ must be treated differently. The conventional method to provide a well posed boundary condition is to impose $p = p_\infty$ at the outflow boundary. This treatment however will create acoustic wave reflections, which may be diffused and eventually disappear when the solution is converged to a steady state solution. For unsteady flows, the wave reflection may contaminate the flow solutions. To avoid wave reflections, the following soft boundary condition was suggested by Rudy-Strikwerda[12] and used by Poinsot-Lele[1].

$$\mathcal{L}_5 = \mathcal{K}(p - p_e) \tag{41}$$

where $\mathcal{K}$ is a constant and is determined by $\mathcal{K} = \sigma(1 - \mathcal{M}^2)c/L$ as given by Poinsot and Lele in [1] for Cartesian coordinates. The corresponding form used in the generalized coordinates is

$$\mathcal{K} = \sigma|1 - \mathcal{M}^2|/(\sqrt{2}J\rho L) \tag{42}$$

where $\mathcal{M}$ is the maximum Mach number in the flow field. L is the characteristic length of the domain. c is the speed of sound. The preferred range for constant σ is 0.2-0.5. The absolute value of $1-\mathcal{M}^2$ is to ensure the term is positive because the maximum Mach number can be greater than 1 in a transonic flow field.

If $\mathcal{L}_5 = 0$, it switches to the 'perfect' non-reflective boundary condition. However, this boundary condition is not well posed and will not lead the solution to the one matching the exit pressure p_∞. Equation (41) assumes that the constant exit pressure p_∞ is imposed at infinity. There exists reflection if $p \neq p_\infty$, which is needed for the well posedness of the numerical solution. For the unsteady problems, Equation (41) will make the mean value of the pressure at the exit very close to p_∞. However, the pressure at the individual control volume may not be exactly equal to p_∞ even though the value of $\mathcal{L}_5$ can be very small. In this sense, Equation (41) may be considered as "almost non-reflective boundary conditions".

The complete boundary conditions used at the exit are the pressure at infinity for Equation (41) and three zero gradient viscous conditions:

$$\frac{\partial}{\partial \xi}\left(\xi_x \tau_{xy} + \xi_y \tau_{yy} + \xi_z \tau_{zy}\right) = 0 \tag{43}$$

$$\frac{\partial}{\partial \xi}\left(\xi_x \tau_{xz} + \xi_y \tau_{yz} + \xi_z \tau_{zz}\right) = 0 \tag{44}$$

$$\frac{\partial}{\partial \xi}\left(\xi_x Q_x + \xi_y Q_y + \xi_z Q_z\right) = 0 \tag{45}$$

The amplitudes of the outgoing characteristic waves, $\mathcal{L}_1$, $\mathcal{L}_2$, $\mathcal{L}_3$, and $\mathcal{L}_4$ are computed from the interior domain. All the conservative variables at phantom points are obtained by solving the characteristic N-S equations, Equation (37). All the transverse and viscous terms in Equation (37) can be evaluated in the same way as the inner domain control volumes. The Roe's Riemann solver is also used for computing fluxes $\mathbf{F}'$ and $\mathbf{G}'$, central differencing is used for fluxes $\mathbf{E}'_v$, $\mathbf{F}'_v$, $\mathbf{F}'_v$. This strategy makes maximum use of the existing code and minimizes the programming work to implement the boundary conditions.

4.3 Subsonic inflow boundary conditions

At $\xi = 1$ boundary, four characteristic waves, $\mathcal{L}_1$, $\mathcal{L}_2$, $\mathcal{L}_3$, and $\mathcal{L}_4$ are entering the domain while $\mathcal{L}_5$ is leaving the domain. For 3-D open field flow cases, four physical boundary conditions are needed, i.e. u_o, v_o, w_o and ρ_o are set to be constant. Other primitive variables are specified according to the freestream condition. The total energy ρe_o is obtained by solving the energy equation in Equation (37). The outgoing wave $\mathcal{L}_5$ can be estimated by using interior variables. The rest of the waves are evaluated by using the LODI relations, Equation (38). $\mathcal{L}_1$ - $\mathcal{L}_4$ can be expressed as

$$\mathcal{L}_1 = -\tilde{\xi}_x \frac{\rho}{\sqrt{2}c}(\mathcal{L}_4 + \mathcal{L}_5), \quad \mathcal{L}_2 = -\tilde{\xi}_y \frac{\rho}{\sqrt{2}c}(\mathcal{L}_4 + \mathcal{L}_5), \quad \mathcal{L}_3 = -\tilde{\xi}_z \frac{\rho}{\sqrt{2}c}(\mathcal{L}_4 + \mathcal{L}_5), \quad \mathcal{L}_4 = \mathcal{L}_5 \tag{46}$$

4.4 Adiabatic wall boundary conditions

At a 3-D adiabatic wall (η = constant), the no-slip condition is enforced by extrapolating the velocity between the phantom and interior cells, $u_o = -u_i$, $v_o = -v_i$, and $w_o = -w_i$. One more physical boundary condition to be imposed on the wall is the adiabatic condition, $\frac{\partial T}{\partial \eta} = 0$. From the adiabatic condition, the ρ_o can be expressed as the following

$$\frac{p_o}{\rho_o} = \frac{p_i}{\rho_i} \tag{47}$$

The total energy ρe_o is determined by solving the energy equation in Equation (37). Then using Equation (47) and Equation (12), ρ_o and p_o can be solved. Cross a η boundary, vector $\mathcal{L}$ is expressed as the following:

$$\mathcal{L} = \begin{pmatrix} \mathcal{L}_1 \\ \mathcal{L}_2 \\ \mathcal{L}_3 \\ \mathcal{L}_4 \\ \mathcal{L}_5 \end{pmatrix} = \begin{pmatrix} V[\tilde{\eta}_x \frac{\partial}{\partial \eta}(\frac{\rho}{J}) + \tilde{\eta}_z \frac{\partial}{\partial \eta}(\frac{v}{J}) - \tilde{\eta}_y \frac{\partial}{\partial \eta}(\frac{w}{J}) - \frac{\tilde{\eta}_x}{c^2}\frac{\partial}{\partial \eta}(\frac{p}{J})] \\ V[\tilde{\eta}_y \frac{\partial}{\partial \eta}(\frac{\rho}{J}) - \tilde{\eta}_z \frac{\partial}{\partial \eta}(\frac{u}{J}) + \tilde{\eta}_x \frac{\partial}{\partial \eta}(\frac{w}{J}) - \frac{\tilde{\eta}_y}{c^2}\frac{\partial}{\partial \eta}(\frac{p}{J})] \\ V[\tilde{\eta}_z \frac{\partial}{\partial \eta}(\frac{\rho}{J}) + \tilde{\eta}_y \frac{\partial}{\partial \eta}(\frac{u}{J}) - \tilde{\eta}_x \frac{\partial}{\partial \eta}(\frac{v}{J}) - \frac{\tilde{\eta}_z}{c^2}\frac{\partial}{\partial \eta}(\frac{p}{J})] \\ (V+C)[\frac{\tilde{\eta}_x}{\sqrt{2}}\frac{\partial}{\partial \eta}(\frac{u}{J}) + \frac{\tilde{\eta}_y}{\sqrt{2}}\frac{\partial}{\partial \eta}(\frac{v}{J}) + \frac{\tilde{\eta}_z}{\sqrt{2}}\frac{\partial}{\partial \eta}(\frac{w}{J}) + \beta\frac{\partial}{\partial \eta}(\frac{p}{J})] \\ (V-C)[-\frac{\tilde{\eta}_x}{\sqrt{2}}\frac{\partial}{\partial \eta}(\frac{u}{J}) - \frac{\tilde{\eta}_y}{\sqrt{2}}\frac{\partial}{\partial \eta}(\frac{v}{J}) - \frac{\tilde{\eta}_z}{\sqrt{2}}\frac{\partial}{\partial \eta}(\frac{w}{J}) + \beta\frac{\partial}{\partial \eta}(\frac{p}{J})] \end{pmatrix} \tag{48}$$

where $V = \eta_x u + \eta_y v + \eta_z w$ and $C = c\beta_\eta$, $\beta_\eta = \sqrt{{\eta_x}^2 + {\eta_y}^2 + {\eta_z}^2}$. It can be seen from Equation (48), the characteristic waves $\mathcal{L}_1$ - $\mathcal{L}_3$ vanish since $V = 0$ at wall surface. At lower wall ($\eta = 1$), the outgoing characteristic wave $\mathcal{L}_5$ is computed from the interior domain. The incoming wave $\mathcal{L}_4$ is estimated by using LODI relations. By solving 2nd - 4th equations in Equation (38), it yields $\mathcal{L}_4$ = $\mathcal{L}_5$. At upper wall (maximum η), the $\mathcal{L}_4$ becomes the outgoing wave, and it can be computed from the interior domain. $\mathcal{L}_5$ is the incoming wave which is evaluated by $\mathcal{L}_5 = \mathcal{L}_4$.

5 Results and Discussion

5.1 A Vortex propagating through a outflow boundary

The first test case is a subsonic vortex propagating flow in an open flow field. The computed domain is rectangular with an inflow and outflow boundary at the inlet and exit and far filed boundaries on the upper and lower border. In [1], a supersonic vortex propagating flow is chosen. It is known that a subsonic vortex propagating flow is more difficult to deal with since the disturbance propagates both upstream and downstream. To test present method under more general conditions, the subsonic vortex propagating flow is selected for this study.

The computational mesh has a length of 2 units in streamwise direction which is 30 degrees to the x direction, while the width is 4 units in transverse direction. The mesh dimensions are 60×100. The laminar Navier-Stokes equations is solved for this flow with $M = 0.8$ and Reynolds Number of 300.

A vorticity is initially located at the center of the domain when dimensionless time $t^* = 0$, and convected downstream toward the outflow boundary. The velocity flow field is initially specified as

$$\begin{pmatrix} u \\ v \end{pmatrix} = \begin{pmatrix} u_\infty \\ v_\infty \end{pmatrix} + \begin{pmatrix} \frac{\partial \psi}{\partial y} \\ -\frac{\partial \psi}{\partial x} \end{pmatrix} \tag{49}$$

$$\psi = C_v exp\left(-\frac{x^2+y^2}{2R_c^2}\right) \tag{50}$$

where u_∞ and v_∞ are the velocity components of the incoming flow, C_v is the coefficient that determines the vortex strength of the velocity field, and R_c is the vortex radius. The total energy field is initialized as

$$\rho e = \rho e_\infty + \rho \frac{C_e^2}{R_c^2} exp\left(-\frac{x^2+y^2}{2R_c^2}\right) \tag{51}$$

where C_e is the coefficient that determines the vortex strength of the total energy field. Equations (49) and (51) are adopted from those used by Poinsot and Lele[1]. The coefficients C_v and C_e, and radius R_c are defined by

$$C_v/(cL) = -0.0005, \quad C_e/(cL) = -0.02, \quad R_c = 0.15 \tag{52}$$

The inflow and outflow boundary conditions used in this case are described in previous section. The far field upper and lower boundaries are treated as perfect non-reflective outflow boundary.

The flow field at inflow boundary is initially set to be uniform. The direction of the incoming flow is parallel to the constant η lines. Obviously, at the inflow boundary, the transverse flux and viscous terms are very small. The error caused by LODI relations is very small and negligible.

To compare the present NRBC with the conventional boundary conditions (CBC) for subsonic flow simulations, the first computation is carried out with CBC, which include: at inflow boundary, u_o, v_o, ρ_o are given such that the streamwise velocity component is uniformly distributed and the transverse velocity component is equal to zero. The pressure is extrapolated from the interior domain, $p_o = p_i$. Then the total energy ρe_o can be computed from the equation of state. At outflow boundary, all the primitive variables are extrapolated from the inner domain except the pressure is set to be constant.

The same case with the same initial flow condition is then calculated using the NRBC developed in present study. Figures 1 and 2 show the computed density contours at four instants by CBC and NRBC respectively. It can been seen from figure 1 that the flow field is seriously distorted by the reflective waves when the vortex propagates through the exit boundary. But there is no noticeable distortion in the solution calculated using NRBC as shown in figure 2. The vortex passes through the outflow NRBC very smoothly. Figures 3 and 4 show the relative streamwise velocity component, $(u^\tau - u^\tau{}_\infty)/u^\tau{}_\infty$ contours at the same four instants by CBC and NRBC respectively. The same phenomenon is observed.

5.2 Inlet-Diffuser Flow

To test the non-reflective boundary conditions for realistic engineering problems. A transonic inlet-diffuser with shock wave boundary layer interaction [13] is computed to demonstrate the advantage of the NRBC.

5.2.1 Steady State Solutions

The steady state solution of the inlet diffuser is calculated first to verify that the NRBC is consistent with the steady state flow. The Reynolds Number is 3.45×10^5 and the inlet Mach number is 0.46.

The baseline geometry of the inlet diffuser has a height of $H = 4.4cm$ at the throat and a total length of $12.6H$. This case is run using a H-type grid with the dimensions of 110×56. The turbulence shear stress and heat flux are calculated by the Baldwin-Lomax model[8]. The experimental data provided by Bogar et al.[13] are available for validation.

As discussed before, for 3-D case, at $\xi = 1$ inlet boundary, waves $\mathcal{L}_1$ - $\mathcal{L}_4$ enter the boundary and $\mathcal{L}_5$ leaves. Hence four physical boundary conditions are required at this boundary. The amplitude of the outgoing characteristic wave $\mathcal{L}_5$ can be estimated from the interior points.

According to [1], the inlet and wall NRBC are not as critical as the exit NRBC. For this transonic inlet-diffuser case, at the upstream of the shock, the flow is supersonic. Hence the perturbation will not propagate upstream. The NRBC at inlet therefore may not be necessary. The CBC at inlet is expected to work well. However, at the downstream of the shock, the flow is subsonic. The oscillation of the shock will generate strong reflecting waves at the exit boundary. Therefore exit NRBC is essential for this case. For this reason, the inflow NRBC is not used in this study. Instead, the conventional inlet BC with given total pressure P_t, total temperature T_t, and flow angle is used. The NRBC outflow and wall conditions used are those described in previous section.

The $Mach$ number contours are shown in Figure 5. Corresponding to different back pressure in the experiment, there are two cases of the flow, one has a weak shock (p_{outlet}/p_t=0.82) and the other has a strong shock (p_{outlet}/p_t=0.72). Fig. 6 and 7 are the computed static pressure distribution compared with the experiment along the top and bottom wall for the weak shock case. Good agreement is obtained between the computation and experiment.

Figures 8 and 9 are the static pressure distribution compared with the experimental data along the top and bottom walls for the strong shock case. Due to the strong shock interacting with the turbulent boundary layer, there is a separation downstream of the shock, which is not well predicted. There may be two reasons for the problem: 1) the flow is unsteady due to the separation and hence the steady state solution can not capture the separation bubble length correctly; 2) the Baldwin-Lomax turbulence model is inadequate to handle the non-equilibrium separated flow.

Different σ values from 0.1 to 0.35 are tested and the results show that the steady state results are insensitive to the σ value. The conventional boundary conditions are also applied to the same case, and achieve almost the same results as the one computed by the NRBC. This is because that, for the steady state solutions, the reflective waves are eventually diffused when the steady state solution is converged.

5.2.2 Unsteady Solutions

The steady state calculation indicates that the NRBC is not essential since the artificial reflective waves are diffused when the solution is converged. However, it is very different when the unsteady flow is calculated. For the inlet-diffuser case with a strong shock wave, the conventional boundary conditions generates strong reflective waves and makes the shock wave severely oscillating inside the duct. The oscillation is far greater than the experimental results. When the NRBC is applied, the shock oscillation is dramatically reduced.

Figures 10 and 11 are the time averaged pressure distributions compared with the experimental data. Due to the large shock oscillation, the shock location is smeared out for the conventional boundary conditions. Hence the shock location, strength and the pressure downstream of the shock are poorly predicted. When the NRBC is applied, the reduced shock oscillation yields sharp shock profile and much better agreement of the shock location with the experiment.

To match the experimental geometry for the measured shock oscillation frequency, the computational domain is then extend to a total length of $21.3H$. The simulation is carried out with CBC and NRBC respectively using the same flow conditions. The computed power spectra for the static pressure at the exit location ($x/H = 14.218$) are shown in Figure 12. The experimental spectrum of the shock oscillation measured for this case only has one dominant frequency between 210 - 225 (Hz)[13]. From the upper spectrum computed by CBC in the figure, it can be seen that the dominant frequencies are 250 (Hz) and 400 (Hz). Obviously the dominant frequency is associated with the reflecting waves. The lower spectrum computed by NRBC shows that there is only one significantly dominant frequency (about 250 Hz) which is very closed to the experimental result. Also it is evident that the noise level created by NRBC is much lower than the one created by CBC. This shows that the NRBC is essential to accurately predict unsteady aerodynamic forcing.

6 Conclusion

The non-reflective boundary conditions of Poinsot and Lele[1] for 3D Navier-Stokes equations are extended to the generalized coordinates in this paper. The NRBC is applied numerically in an implicit time marching method. The governing equations for inner domain and NRBC are solved simultaneously in a fully couple manner.

For the unsteady subsonic vortex propagating flow, the conventional boundary conditions imposing the exit pressure generates serious wave reflection and the flow field is distorted, whereas, the NRBC developed in this paper generates clean results with no wave reflection and solution distortion.

For the transonic inlet-diffuser, the NRBC is not necessary for steady state solutions since the reflective waves are diffused when the solutions are converged. However, for unsteady flows, the NRBC is essential. The conventional boundary conditions generate strong reflective waves due to the shock/boundary layer interaction, which makes the shock oscillating motion far greater than the experiment. When the NRBC is applied, the shock oscillation is dramatically reduced and the computed time averaged pressure distributions and frequency agree much better with the experiment than CBC.

7 Acknowledgment

This work is supported by AFOSR Grant F49620-03-1-0253 monitored by Dr. Fariba Fahroo.

References

[1] T. Poinsot and S. Lele, " Boundary Conditions for Direct Simulations of Compressible Viscous Flows," *Journal of Computational Physics*, vol. 101, pp. 104–129, 1992.

[2] T. Nishizawa and H. Takata, " Numerical Study on Rotating Stall in Finite Pitch Cascades." ASME Paper., Proceedings of the International Gas Turbine and Aeroengine Congress and Exposition, The Hague, Netherlands, June 1994.

[3] L. He, " Computational Study of Rotating Stall Inception in Axial Compressors," *Journal of Propulsion and Power*, vol. 13, pp. 31–38, 1997.

[4] M. Giles, "Nonreflecting Boundary Conditions for Euler Calculations ," *AIAA Journal*, vol. 28, No. 12, pp. 2050–2058, 1990.

[5] J. W. Kim and D. J. Lee, "Generalized Characteristic Boundary Conditions for Computational Acoustics," *AIAA Journal*, vol. 38, pp. 2040–2049, 2000.

[6] G. B. Whitham, *Linear and Nonlinear Waves.* Wiley, New York, 1974.

[7] K. Thompson, "Time Dependent Boundary Conditions for Hyperbolic Systems," *Journal of Computational Physics*, vol. 68, 1987.

[8] B. Baldwin and H. Lomax, "Thin Layer Approximation and Algebraic Model for Separated Turbulent Flows." AIAA Paper 78-257, 1978.

[9] A. Jameson, "Time Dependent Calculations Using Multigrid with Application to Unsteady Flows past Airfoils and Wings." AIAA Paper 91-1596, 1991.

[10] P. Roe, "Approximate Riemann Solvers, Parameter Vectors, and Difference Schemes," *Journal of Computational Physics*, vol. 43, pp. 357–372, 1981.

[11] B. Van Leer, "Towards the Ultimate Conservative Difference Scheme, III," *Journal of Computational Physics*, vol. 23, pp. 263–75, 1977.

[12] D. Rudy and J. Strikwerda, "A Nonreflecting Outflow Boundary Condition for Subsonic Navier-Stokes Calculations," *Journal of Computational Physics*, vol. 36, pp. 55–70, 1980.

[13] T. Bogar, M. Sajben, and J. Kroutil, "Characteristic Frequency and Length Scales in Transonic Diffuser Flow Oscillations." AIAA Paper 81-1291, 1981.

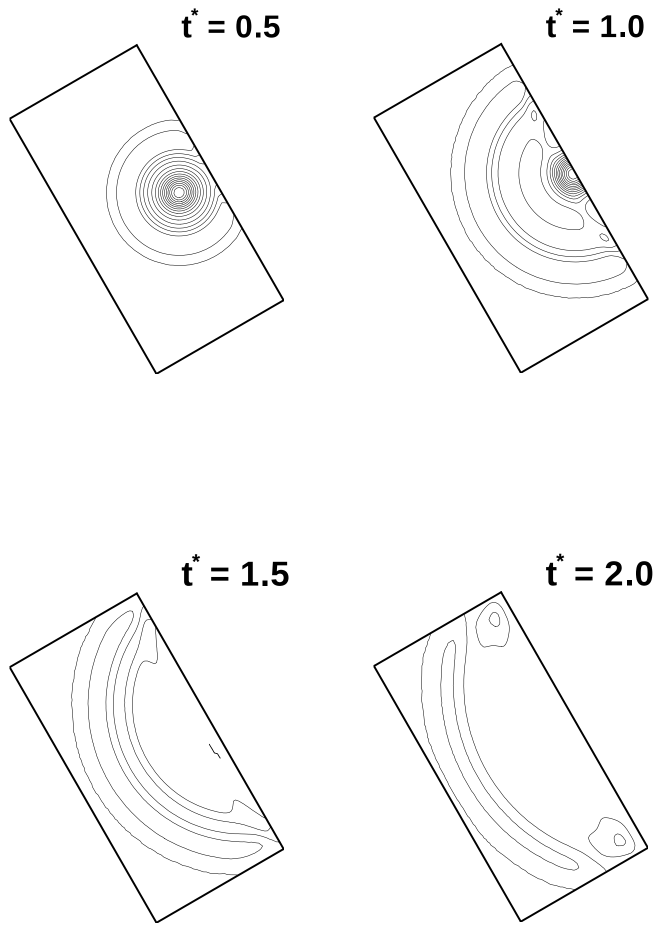

Figure 1: Density contours at four instants for a vortex leaving the domain using imposed exit static pressure boundary conditions.

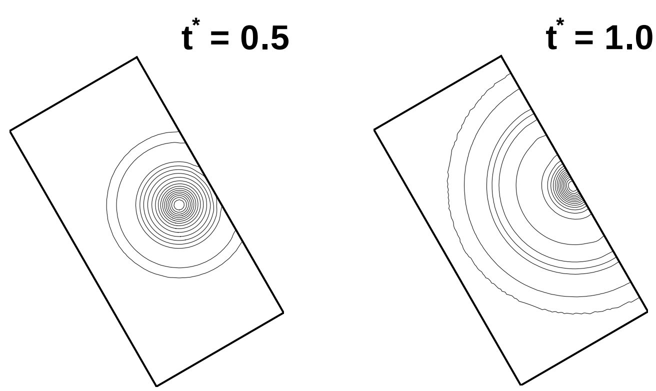

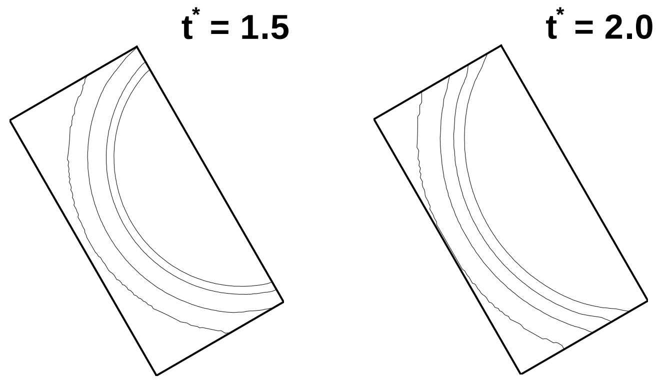

Figure 2: Density contours at four instants for a vortex leaving the domain using NRBC exit boundary conditions.

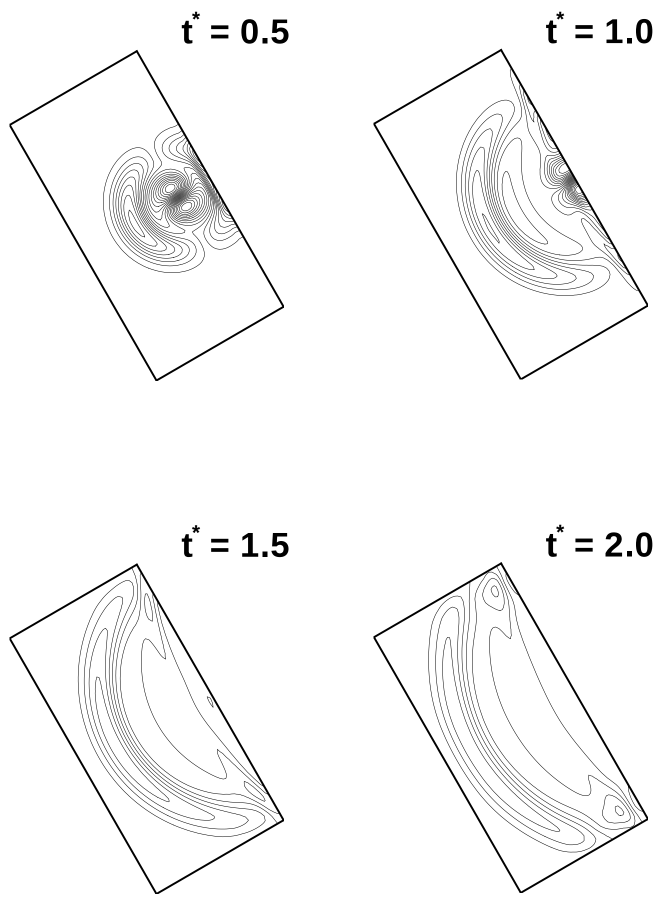

Figure 3: $(u^\tau - u^\tau{}_\infty)/u^\tau{}_\infty$ contours at four instants for a vortex leaving the domain using imposed exit static pressure boundary conditions.

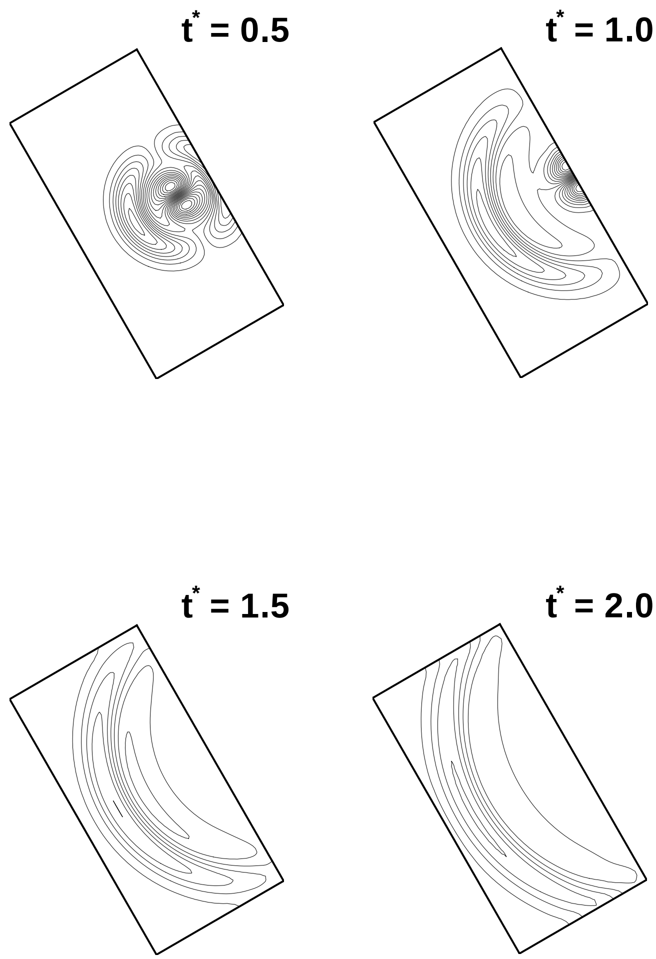

Figure 4: $(u^\tau - u^\tau{}_\infty)/u^\tau{}_\infty$ contours at three instants for a vortex leaving the domain using NRBC exit boundary conditions.

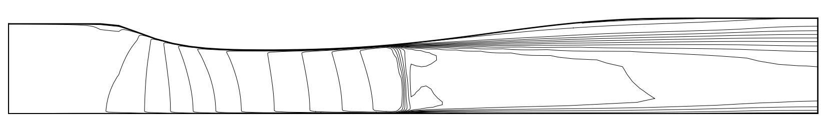

Figure 5: $Mach$ number contours of the inlet diffuser.

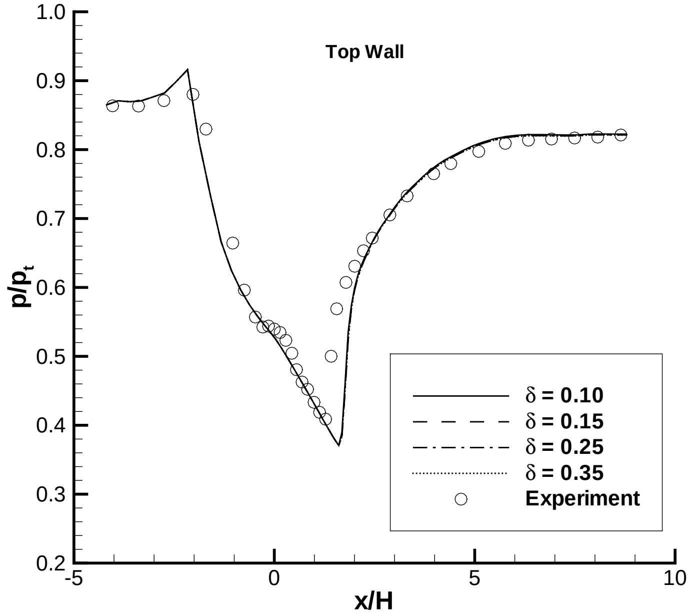

Figure 6: Steady state pressure distribution along the top wall for $p_{outlet}/p_t = 0.82$.

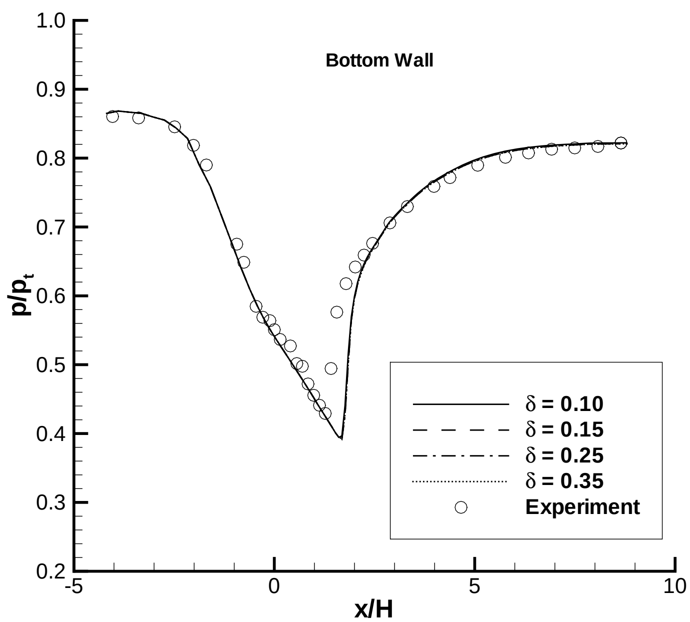

Figure 7: Steady state pressure distribution along the bottom wall for $p_{outlet}/p_t = 0.82$.

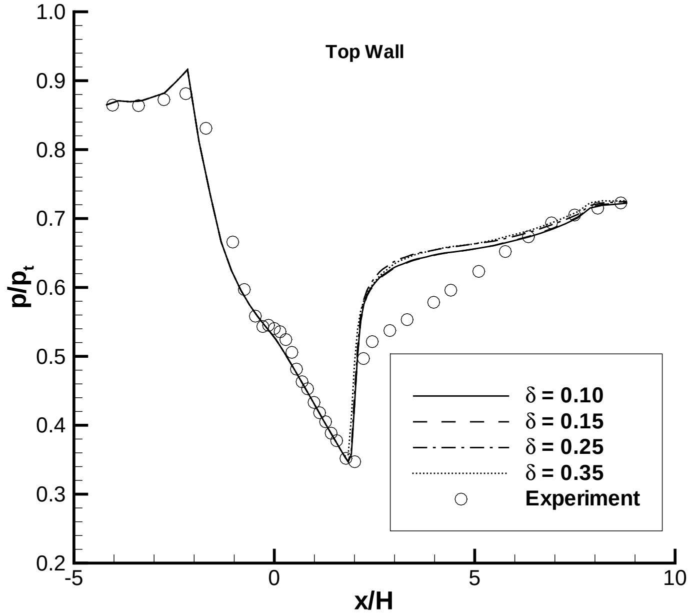

Figure 8: Steady state pressure distribution along the top wall for $p_{outlet}/p_t = 0.72$.

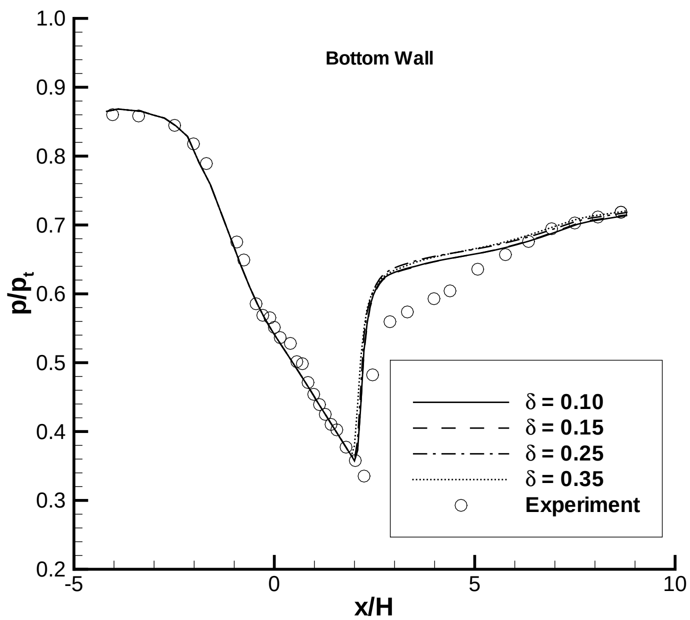

Figure 9: Steady state static pressure distribution along the bottom wall for $p_{outlet}/p_t = 0.72$.

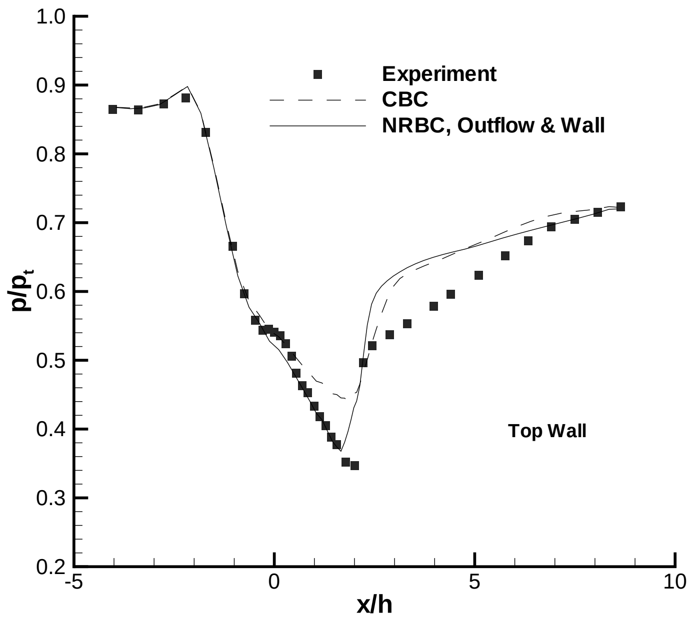

Figure 10: Time averaged unsteady pressure distribution along the top wall for $p_{outlet}/p_t = 0.72$.

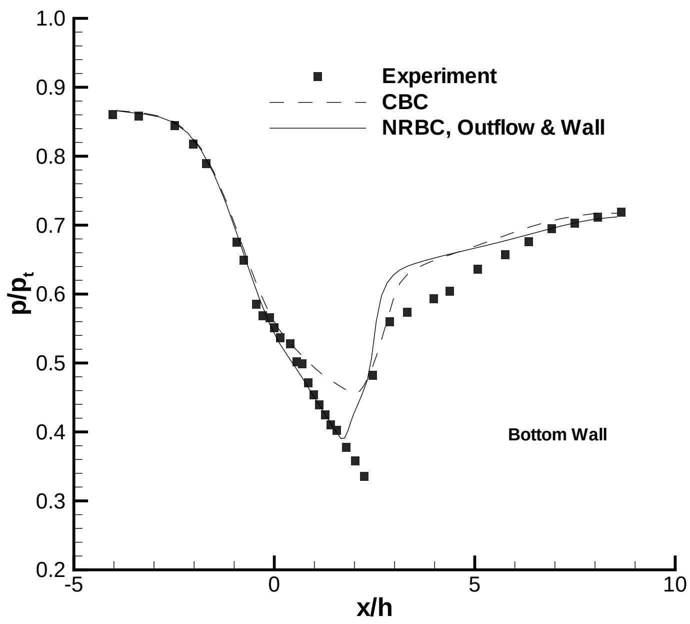

Figure 11: Time averaged unsteady pressure distribution along the bottom wall for $p_{outlet}/p_t = 0.72$.

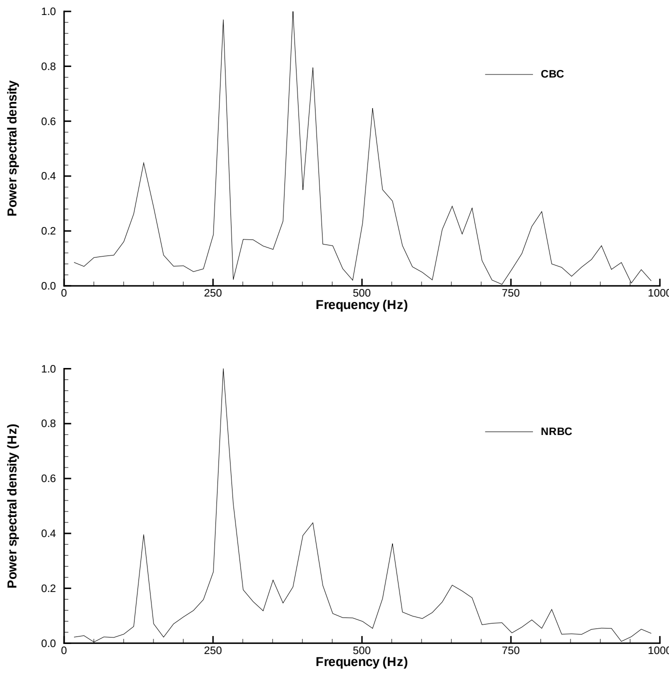

Figure 12: Power spectral density for the static pressure fluctuations at $x/H = 14.218$, $p_{outlet}/p_t = 0.72$.